

Journal of Geophysical Research: Space Physics

RESEARCH ARTICLE

10.1002/2017JA024489

Key Points:

- Geomagnetic storms lead to H redistribution in the geocorona, exhibiting as evident changes in the H emissions relative to quiet times
- Ion-neutral interactions in the topside ionosphere and inner plasmasphere are postulated to be the primary driver of the H redistribution
- Geocoronal H emissions potentially could be used to monitor geomagnetic storms and the related upper atmospheric coupling effects

Correspondence to:

J. Qin,
jianqi@illinois.edu

Citation:

Qin, J., L. Waldrop, and J. J. Makela (2017), Redistribution of H atoms in the upper atmosphere during geomagnetic storms, *J. Geophys. Res. Space Physics*, 122, 10,686–10,693, doi:10.1002/2017JA024489.

Received 19 JUN 2017

Accepted 9 AUG 2017

Accepted article online 14 AUG 2017

Published online 23 OCT 2017

Redistribution of H atoms in the upper atmosphere during geomagnetic storms

Jianqi Qin¹ , Lara Waldrop¹ , and Jonathan J. Makela¹ ¹Department of Electrical and Computer Engineering, University of Illinois at Urbana-Champaign, Urbana, Illinois, USA

Abstract Geocoronal H emission data acquired by NASA's Thermosphere Ionosphere Mesosphere Energetics and Dynamics mission are analyzed to quantify the H density distribution over the entire magnetosphere-ionosphere-thermosphere region in order to investigate the response of the atmospheric system as a whole to geomagnetic storms. It is shown that at low and middle latitudes the H density averaged over storm times in the thermosphere-exosphere transition region decreases by ~30%, while the H density at exospheric altitudes above $\sim 1\text{--}2 R_E$ increases by up to ~40% relative to quiet times. We postulate that enhanced ion-neutral charge exchange in the topside ionosphere and inner plasmasphere is the primary driver of the observed H redistribution. Specifically, charge exchange reactions between H atoms and ionospheric/plasmaspheric O⁺ lead to direct H loss, while those between thermal H and H⁺ yield kinetically energized H atoms which populate gravitationally bound satellite orbits. The resulting H density enhancements in the outer exosphere would enhance the charge exchange rates in the ring current and the associated energetic neutral atom production. Regardless of the underlying mechanisms, H redistribution should be considered as an important process in the study of storm time atmospheric evolution, and the resultant changes in the geocoronal H emissions potentially could be used to monitor geomagnetic storms.

1. Introduction

Geomagnetic storms are temporal disturbances in the Earth's magnetosphere due to sudden and drastic increase of solar wind energy input into the terrestrial atmospheric system. Over the past few decades, it has been well established that geomagnetic storms can significantly affect the near-Earth space environment, leading to enhancement of ionospheric plasma densities [Foster and Rideout, 2005; Heelis et al., 2009; Immel and Mannucci, 2013], compression of the plasmasphere [Spasojevic et al., 2003; Huba and Krall, 2013], and heating of the thermosphere [Fuller-Rowell et al., 1994; Burns et al., 1995; Lei et al., 2010]. Variations of the atmospheric temperature, composition, and particle densities during storms can manifest as evident changes in the observations of thermospheric UV emissions [Stephan et al., 2000; Zhang et al., 2006] and exospheric H emissions [Kerr et al., 2001; Bailey and Gruntman, 2013; Kuwabara et al., 2017; Zouennchen et al., 2017].

In particular, middle- and low-latitude thermospheric UV emissions, such as the H Ly α 121.6 nm, OI 130.4 nm, and OI 135.6 nm emissions, observed from nadir-viewing satellites in low Earth orbit (~ 600 km) have been shown to increase significantly during geomagnetic storms [e.g., Stephan et al., 2000, 2001; Zhang et al., 2006]. Moreover, recent analyses of the data obtained from the Two Wide-angle Imaging Neutral-atom Spectrometers (TWINS) mission have revealed that the H Ly α emission at $\sim 2\text{--}7 R_E$ altitudes is also enhanced markedly during geomagnetic storms, indicating an increase of H density in this exospheric region [Bailey and

This website utilizes technologies such as cookies to enable essential site functionality, as well as for analytics, personalization, and targeted advertising. You may change your settings at any time or accept the default settings. You may close this banner to continue with only essential cookies. [Privacy Policy](#)

[Manage Preferences](#)[Accept All](#)[Reject All](#)

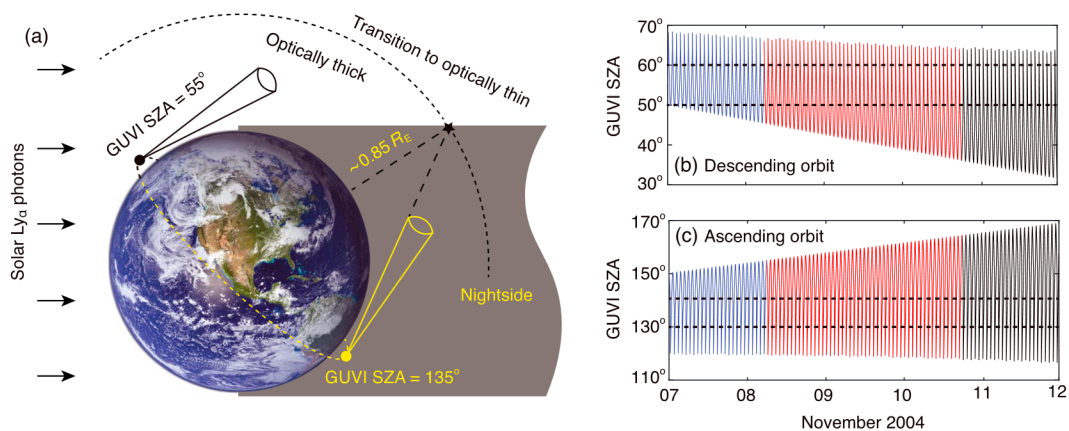


Figure 1. (a) A diagram of the TIMED/GUVI limb scanning geometry. When satellite solar zenith angle (SZA) = 55°/135°, the limb scans are sensitive to the conditions below/above ~ 5400 km altitude ($\sim 0.85 R_E$), assuming a shadow height of ~ 100 km (b, c) SZA of the descending and ascending orbits during the time period of 7–11 November 2004. Blue, red, and black colors correspond to the time periods before, during, and after the storm event analyzed in Figures 2a–2d.

storm times. Enhanced ion-neutral interactions in the topside ionosphere and inner plasmasphere are postulated to be the primary driver of the observed H redistribution. These processes would lead to H depletion in the transition region while enhancing the H density in the outer exosphere, manifesting optically as evident changes in geocoronal H emissions that potentially could be used to monitor geomagnetic storms.

2. Instrument and Model

The TIMED satellite is the first mission of the NASA Solar Connections program and was launched in 2001 into a nearly circular orbit at 625 km altitude with an inclination of 74° from the equator. The GUVI's 11.78° field of view is mapped into 14 spatial pixels along the spacecraft orbital track and 160 spectral bins spanning 115 to 180 nm. Multispectral images spanning the Earth's full disk to the antisunward limb are generated by sweeping the field of view from horizon to horizon perpendicular to the spacecraft motion using a scan mirror. The limb scanning portion of the image is binned into 32 pixels, corresponding to lines of sight having local zenith angles of $\sim 100^\circ$ – 112° and tangent point altitudes of ~ 520 – 110 km [Christensen et al., 2003]. The measured spectrum is binned by an onboard detector processor into five distinct wavelength intervals in each of the 14 along-track and 32 cross-track spatial bins of the limb images. Additional data processing steps include pointing calibration using stellar sources and brightness calibration that accounts for background and scattered light contamination. We combine overlapping along-track samples from three consecutive images as a moving average in order to increase the signal-to-noise ratio associated with each scan (see Waldrop and Paxton [2013] for details.)

The geocoronal H Ly α emission is produced by resonant scattering of solar Ly α photons. Since GUVI views the antisunward limb, detected Ly α photons can all be attributed to resonant scattering. As a result, the Ly α radiance profile across the limb depends sensitively on the underlying H distribution. Estimation of H density from the limb scans requires the use of a nonisothermal radiative transfer model, which has been developed for interpretation of UV photon scattering by H atoms in the atmosphere assuming spherical symmetry of the H density distribution, cylindrical symmetry of the Ly α emission with respect to the Sun-Earth line,

This website utilizes technologies such as cookies to enable essential site functionality, as well as for analytics, personalization, and targeted advertising. You may change your settings at any time or accept the default settings. You may close this banner to continue with only essential cookies. [Privacy Policy](#)

[Manage Preferences](#)

[Accept All](#)

[Reject All](#)

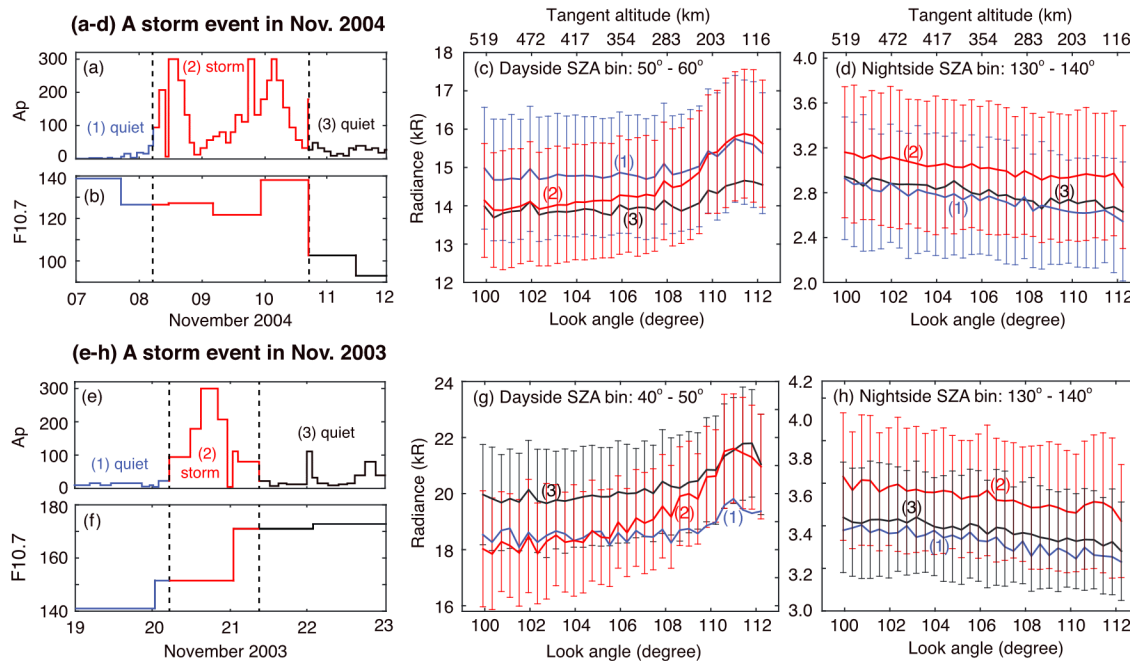


Figure 2. (a–d) Analysis of a storm that occurred in 8–10 November 2004. Figures 2a and 2b show the Ap and $F_{10.7}$ indices, respectively. Figure 2c shows the dayside Ly α limb scan radiances binned and averaged over SZA = 50° – 60° for the (1) prestorm, (2) storm time, (3) poststorm period. The vertical bars show the standard deviations of the scans that are binned and averaged in each case. Look angle is the polar angle of the lines of sight with respect to the local spacecraft zenith direction, and tangent altitude is the height of the tangent point of the lines of sight. Figure 2d shows the nightside limb scans binned and averaged over SZA = 130° – 140° . (e–h) Analysis of another storm that occurred in 20–21 November 2003.

solar photons scattered from the low-altitude sunlit dusk/dawn region need to pass through an optically thick thermospheric region in the nightside before they can reach the space volume within the GUVI field of view and then be scattered into the instrument, while those photons scattered by H atoms that are located in the high-altitude (above $\sim 0.85 R_E$ altitude; see Figure 1a) sunlit region within the GUVI field of view have an optically much shorter path in the thermosphere to go through before reaching GUVI. Since both day-side and nightside scans acquired on the same orbit sample a common high-altitude exospheric region that is poorly constrained by the dayside scans (see Figure 1a), nightside scans are used as additional constraints to improve the accuracy of the estimation at high altitudes under the assumption of a spherically symmetric H distribution. Similar to previous analyses, we incorporate physically derived, parameterized H density profiles to guarantee solution uniqueness and solve the inverse problem by determining the optimal parameters associated with the best fit of the model to the normalized Ly α limb profile data in the least squares sense. The H density profiles are parameterized using the two-exponential model proposed by Qin and Waldrop [2016] combined with the analytical model used by Bishop [1999].

3. Geomagnetic Storm Effects on the Geocoronal H Ly α Emission

We first examine individual storms which occurred during 2002–2007 by binning and averaging the observed Ly α limb scans spatially over satellite SZA and temporally over the prestorm, storm time, and poststorm

This website utilizes technologies such as cookies to enable essential site functionality, as well as for analytics, personalization, and targeted advertising. You may change your settings at any time or accept the default settings. You may close this banner to continue with only essential cookies. [Privacy Policy](#)

[Manage Preferences](#)

[Accept All](#)

[Reject All](#)

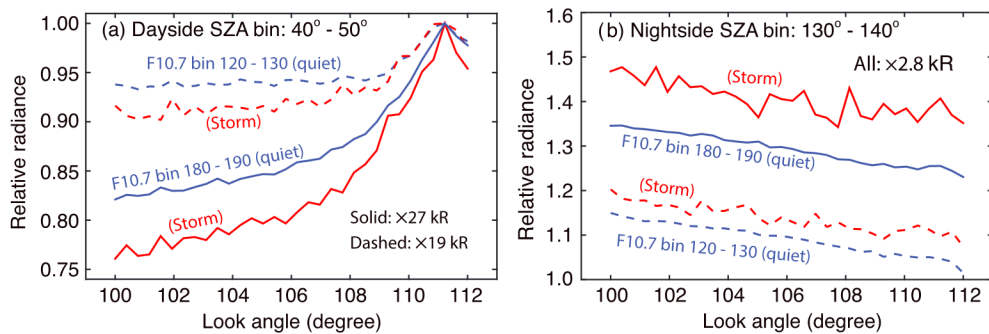


Figure 3. (a) Binned and averaged dayside Ly α limb scans associated with SZA from 40° to 50° . The $F_{10.7}$ binning ranges are from 120 to 130 and 180 to 190. The quiet and storm cases are associated with $Ap \leq 20$ and $60 \leq Ap \leq 150$, respectively. For highlighting the changes in the shape of the radiance profiles, the limb scans have been normalized using a factor of ~ 27 kR and ~ 19 kR for cases of the high and low solar activities, respectively. (b) Binned and averaged nightside Ly α limb scans associated with SZA from 130° to 140° . The normalization factor is chosen to be ~ 2.8 kR, the lowest value of the radiances in the four cases, to allow straightforward comparison of the relative values. Standard deviations of the scans binned in each case (not shown here for clarity of the figure) are similar to those shown in Figure 2.

[Barth *et al.*, 1990]. An important feature revealed in Figure 2c is that the shape of the storm time limb scan is clearly different from that of the quiet time, indicating that the H distribution changes during the storm. Figure 2d shows the nightside limb scans from the same orbit binned and averaged over SZA of 130° – 140° , which exhibit an increase during the storm. Figures 2e–2h present another event that occurred from 20 to 21 November 2003 to demonstrate that the variations in the H Ly α emission shown in Figures 2a–2d are common to all geomagnetic storms observed.

Although the standard deviations shown in Figure 2 are large when compared to the storm-induced changes in the H Ly α emission, the trend of the changes is consistently observed during most of the ~ 20 storms we have analyzed. However, the changes are observed to be less significant for storms associated with lower Ap index. For events associated with $Ap \lesssim 150$, clear changes as those shown in Figure 2 are not always observed. This finding does not necessarily imply that relatively weak storms do not produce discernible changes in the H Ly α emission because the storm effects shown in Figure 2 are averaged over the entire storm period, when the Ap index varies significantly. For less intense storms, a more reliable means of characterizing the storm-induced variability is to analyze composite profiles generated by binning and averaging the limb scan data with respect to satellite SZA, solar $F_{10.7}$ index, and Ap index. Figure 3 presents a typical result of this analysis, depicting composite profiles having SZA ranging from 40° to 50° (dayside) and 130° to 140° (nightside), $F_{10.7}$ ranging from 120 to 130 (low solar activity) and 180 to 190 (high solar activity), and Ap ranging from 0 to 20 (quiet time) and 60 to 150 (storm time). This analysis reveals that the H Ly α emission varies in response to relatively weak storms with the same trend observed during intense storms.

4. Storm-Driven H Redistribution in the Terrestrial Atmosphere

The observed changes in geocoronal H Ly α emission suggest variations of the atmospheric H distribution during storm times. Figure 4 depicts the inversion results associated with the two intense storms presented in Figure 2 using the models described in section 2. To avoid contamination from thermospheric N 120 nm emission which might be significant near ~ 140 – 180 km altitudes [Meier *et al.*, 1980], we use only the part

This website utilizes technologies such as cookies to enable essential site functionality, as well as for analytics, personalization, and targeted advertising. You may change your settings at any time or accept the default settings. You may close this banner to continue with only essential cookies. [Privacy Policy](#)

[Manage Preferences](#)

[Accept All](#)

[Reject All](#)

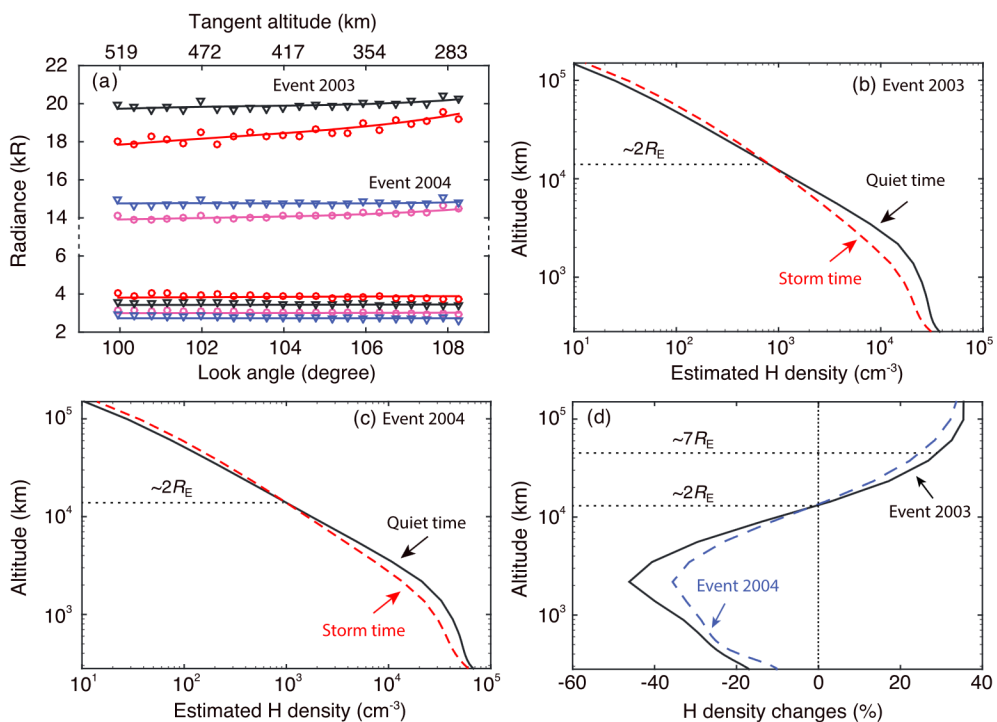


Figure 4. (a) The triangles and circles represent the limb scan data associated with quiet time and storm time, respectively. The solid lines represent the modeled best fit radiances. The top four lines are the dayside scans, whereas the bottom four lines are the nightside ones. (b, c) The retrieved H density profiles leading to the best fits. (d) The percentage differences of the storm time H density with respect to the quiet time H density associated with the (solid) 2003 event and (dashed) 2004 event.

in storm-induced H density changes as intense storms. In that case, however, the density changes are less pronounced in the thermospheric-exospheric transition region, where the peak depletion is reduced to $\sim 20\%$, and the altitude transition between density depletion and enhancement occurs at $\sim 1.2 R_E$ instead of $\sim 2 R_E$.

Quantification of the uncertainties in the retrieved H density profiles requires knowledge about the uncertainties in several physical quantities used in the inversion, such as the H kinetic distribution, the global structure of the geocorona, and the thermospheric O₂ density and neutral temperature, none of which can be readily quantified. Moreover, despite the inclusion of nightside limb scans as additional constraints, the observed radiances from a low Earth orbit vantage are still not sufficiently sensitive for accurate quantification of the H density at altitudes above several Earth radii. Another potential source of uncertainty is our neglect of interplanetary Ly α background emission. The vertical optical depth from GUVI's 625 km altitude to the outer edge of the exosphere is $\sim 1.5 - 2$, such that an interplanetary Ly α emission of ~ 0.7 kR contributes ~ 0.1 kR to the GUVI measurements. We have confirmed that removal of 0.1 kR from the radiances shown in Figure 2 leads to negligible changes in the estimated H density profiles.

A potentially more significant error source arises from the spherically symmetric H density assumption used for the inversion. It is known that the terrestrial H distribution exhibits local time asymmetries, primarily in the

This website utilizes technologies such as cookies to enable essential site functionality, as well as for analytics, personalization, and targeted advertising. You may change your settings at any time or accept the default settings. You may close this banner to continue with only essential cookies. [Privacy Policy](#)

[Manage Preferences](#)

[Accept All](#)

[Reject All](#)

demonstrated that gravitational escape, radiation pressure, and ion-neutral charge exchange lead to deviations from isotropy as well as kinetic energization [Hodges, 1994]. For a given H density profile, a higher effective H temperature leads to larger Ly α radiances. This is because a more energetic H population scatters solar photons in a broader frequency range near the Ly α line center, which results in a broader terrestrial emission line and less attenuation of the solar Ly α flux (i.e., the nearly flat solar emission line diminishes in a broader frequency range near the Ly α line center but with a smaller magnitude when the solar photons pass through the geocorona). Therefore, the exospheric Ly α emission enhancements shown in Figure 2 may arise as a consequence of actual H density enhancement at high altitudes and/or increases in effective temperature due to the storm-induced charge exchange energization of the exospheric H population.

Although we cannot quantify the above-discussed uncertainties due to insufficient data constraints, we note that our results are consistent with previously reported observations. For example, Stephan *et al.* [2000] showed a storm time brightness decrease in the dayside Ly α airglow emission as measured in the near-z zenith direction by the STP 78-1 satellite in low Earth orbit at 600 km. In additional simulations not shown here, we successfully reproduced these observations by modeling upward viewing Ly α measurements from a 600 km vantage using our estimated quiet time and storm time H density profiles. Moreover, increase of H density by ~23% in the exosphere from ~2 to $7 R_E$ altitude during storm times has been reported recently by Zoenenchen *et al.* [2017]. Our inversions associated with this region, marked with two horizontal lines in Figure 4(d), are in good agreement with their TWINS-based estimates. Because of these good agreements and the fact that our results are based on the relative variations rather than the absolute values of the H density, we consider our inversions to be sufficiently accurate to support the interpretation presented in the next section.

5. Implications for Storm-Induced Coupling of the Atmospheric System

Atomic hydrogen is the primary participant of ion-neutral interactions over the vast majority of the volume of geospace, energetically and dynamically coupling the upper atmosphere with the ionosphere, plasmasphere, and magnetosphere. Our ability to quantify the H density distributions over the entire magnetospheric-ionospheric-thermospheric region provides a unique means to investigate the response of the terrestrial atmospheric system as a whole to geomagnetic storms. One of the novel results presented in this study is the significant H depletion in the transition region above ~300 km altitude and below ~1–2 R_E altitude during geomagnetic storms. Although the underlying physical mechanisms of this depletion cannot be determined from the GUVI data alone, we postulate that the changes in the vertical structure of the derived H density are indicative of storm-enhanced ion-neutral coupling. Specifically, a transient decrease in H density can only occur through temporary enhancements in H loss through charge exchange reactions with O⁺ ions (yielding H⁺ and an energetic O atom) and/or a temporary positive divergence of H flux, most likely driven by gradients in horizontal or vertical H velocity. While bulk transport effects cannot be discounted and indeed may be operative in the collisionally dominated thermosphere, plasma densities in the topside ionosphere and inner plasmasphere are well known to be significantly enhanced during geomagnetic storms [Foster and Rideout, 2005; Heelis *et al.*, 2009]. Charge exchange reactions between H atoms and ionospheric/plasmaspheric O⁺ lead to direct H loss as described above, while those between thermal H and H⁺ yield kinetically energized H atoms which follow ballistic trajectories. If moving downward, the hot H atoms enhance the thermospheric H density (and likely the temperature as well, through collisional thermalization), and, if moving upward, they either populate gravitationally bound satellite orbits or escape into interplanetary space [Maher and Tinsley, 1977; Hunten, 1982]. We note that particle conservation is not observed when comparing the quiet time and storm time H density profiles: the total number of H atoms lost in the transition region can only compensate

This website utilizes technologies such as cookies to enable essential site functionality, as well as for analytics, personalization, and targeted advertising. You may change your settings at any time or accept the default settings. You may close this banner to continue with only essential cookies. [Privacy Policy](#)

[Manage Preferences](#)

[Accept All](#)

[Reject All](#)

the same process should also lead to precipitation of hot H and O atoms from the plasmasphere onto the thermosphere, which might be more responsible for the thermospheric UV emission enhancements relative to ENA precipitation.

6. Conclusions

The geocoronal Ly α limb scan data acquired by NASA's TIMED/GUVI instrument are analyzed using a radiative transfer model to quantify the terrestrial H redistribution induced by geomagnetic storms. Comparison of the estimated H density profiles averaged separately over quiet and storm times shows a decrease of the H density by ~40% in the upper thermosphere and the lower exosphere and an increase by up to ~40% in the exosphere above $\sim 1-2 R_E$ altitude during storms. We suggest that storm-enhanced charge exchange of the thermal H and O atoms with the hot H $^+$ and O $^+$ ions in the topside ionosphere and inner plasmasphere between ~ 300 km and $2 R_E$ altitude is the primary driver of the quantified H redistribution. The resulting hot H atoms, if moving downward, precipitate onto the lower thermosphere, and, if moving upward, they either populate the gravitationally bound satellite orbits or escape into interplanetary space. We propose that H redistribution should be considered as an important process in the study of storm time atmospheric evolution.

Acknowledgments

The GUVI data used here (level 1B data products, version 8) are provided through support from the National Aeronautics and Space Administration MO&DA program. The GUVI instrument was designed and built by The Aerospace Corporation and The Johns Hopkins University. The Principal Investigator is Andrew B. Christensen, and the Chief Scientist and co-PI is Larry J. Paxton. This work was supported by the National Aeronautics and Space Administration award NNX16AF77G and by the National Science Foundation award AGS 14-54839 CAR. Requests for data should be directed to J. Q. (jianqi@illinois.edu).

References

- Anderson, D. E., L. J. Paxton, R. P. McCoy, R. R. Meier, and S. Chakrabarti (1987), Atomic hydrogen and solar Lyman alpha flux deduced from STP 78-1 UV observations, *J. Geophys. Res.*, 92, 8759–8766, doi:10.1029/JA092iA08p08759.
- Bailey, J., and M. Gruntman (2013), Observations of exosphere variations during geomagnetic storms, *Geophys. Res. Lett.*, 40, 1907–1911, doi:10.1002/grl.50443.
- Barth, C. A., W. K. Tobiska, G. J. Rottman, and O. R. White (1990), Comparison of 10.7 cm radio flux with SME solar Lyman alpha flux, *Geophys. Res. Lett.*, 17(5), 571–574, doi:10.1029/GL017i005p00571.
- Bishop, J. (1999), Transport of resonant atomic hydrogen emissions in the thermosphere and geocorona: Model description and applications, *J. Quant. Spectrosc. Radiat. Transfer*, 61, 473–491, doi:10.1016/S0022-4073(98)00031-4.
- Burns, A. G., T. L. Killeen, W. Deng, G. R. Carignan, and R. G. Roble (1995), Geomagnetic storm effects in the low- to middle-latitude upper thermosphere, *J. Geophys. Res.*, 100(A8), 14,673–14,691, doi:10.1029/94JA03232.
- Christensen, A. B., et al. (2003), Initial observations with the Global Ultraviolet Imager (GUVI) in the NASA TIMED satellite mission, *J. Geophys. Res.*, 108, 1451, doi:10.1029/2003JA009918.
- Foster, J. C., and W. Rideout (2005), Midlatitude TEC enhancements during the October 2003 superstorm, *Geophys. Res. Lett.*, 32, L12S04, doi:10.1029/2004GL021719.
- Fuller-Rowell, T. J., M. V. Codrescu, R. J. Moffett, and S. Quegan (1994), Response of the thermosphere and ionosphere to geomagnetic storms, *J. Geophys. Res.*, 99(A3), 3893–3914, doi:10.1029/93JA02015.
- Heelis, R. A., J. J. Sojka, M. David, and R. W. Schunk (2009), Storm time density enhancements in the middle-latitude dayside ionosphere, *J. Geophys. Res.*, 114, A03315, doi:10.1029/2008JA013690.
- Hodges, R. R. (1994), Monte Carlo simulation of the terrestrial hydrogen exosphere, *J. Geophys. Res.*, 99, 23,229–23,247, doi:10.1029/94JA02183.
- Huba, J., and J. Krall (2013), Modeling the plasmasphere with SAMI3, *Geophys. Res. Lett.*, 40, 6–10, doi:10.1029/2012GL054300.
- Hunten, D. M. (1982), Thermal and nonthermal escape mechanisms for terrestrial bodies, *Planet Space Sci.*, 30, 773–783, doi:10.1016/0032-0633(82)90110-6.
- Immel, T. J., and A. J. Mannucci (2013), Ionospheric redistribution during geomagnetic storms, *J. Geophys. Res. Space Physics*, 118, 7928–7938, doi:10.1002/2013JA018919.
- Kerr, R. B., et al. (2001), Secular variability of the geocoronal Balmer-alpha brightness: magnetic activity and possible human influences, *J. Geophys. Res.*, 106(A12), 28,819–28,829, doi:10.1029/1999JA900187.
- Kuwabara, M., K. Yoshioka, G. Murakami, F. Tsuchiya, T. Kimura, A. Yamazaki, and I. Yoshikawa (2017), The geocoronal responses to the geomagnetic disturbances, *Geophys. Res. Lett.*, 122, 1269–1276, doi:10.1002/2016JA023247.
- Lei, J. H., J. P. Thayer, A. G. Burns, G. Lu, and Y. Deng (2010), Wind and temperature effects on thermosphere mass density response to the November 2004 geomagnetic storm, *J. Geophys. Res.*, 115, A05303, doi:10.1029/2009JA014754.
- Maher, L. J., and B. A. Tinsley (1977), Atomic hydrogen escape rate due to charge exchange with hot plasmaspheric ions, *J. Geophys. Res.*, 82, 689–695, doi:10.1029/JA082i004p00689.
- Meier, R. R., D. J. Strickland, P. D. Feldman, and E. P. Gentieu (1980), The ultraviolet dayglow 1. Far UV emissions of N and N₂, *J. Geophys. Res.*, 85(NAS), 2177–2184, doi:10.1029/JA085iA05p02177.
- Picone, J. M., A. E. Hedin, D. P. Drob, and A. C. Akin (2002), NRLMSISE-00 empirical model of the atmosphere: Statistical comparisons and scientific issues, *J. Geophys. Res.*, 107(A12), 1458, doi:10.1029/2002JA009120.

This website utilizes technologies such as cookies to enable essential site functionality, as well as for analytics, personalization, and targeted advertising. You may change your settings at any time or accept the default settings. You may close this banner to continue with only essential cookies. [Privacy Policy](#)

[Manage Preferences](#)

[Accept All](#)

[Reject All](#)

- Zhang, Y., L. J. Paxton, J. U. Kozyra, H. Kil, and P. C. Brandt (2006), Nightside thermospheric FUV emissions due to energetic neutral atom precipitation during magnetic superstorms, *J. Geophys. Res.*, 111, A09307, doi:10.1029/2005JA011152.
- Zoennchen, J. H., U. Nass, H. J. Fahr, and J. Goldstein (2017), The response of the H geocorona between 3 and $8 R_e$ to geomagnetic disturbances studied using TWINS stereo Lyman- α data, *Ann. Geophys.*, 35(1), 171–179, doi:10.5194/angeo-35-171-2017.
- Zoennchen, J. H., U. Nass, and H. J. Fahr (2015), Terrestrial exospheric hydrogen density distributions under solar minimum and solar maximum conditions observed by the TWINS stereo mission, *Ann. Geophys.*, 33, 413–426, doi:10.5194/angeo-33-413-2015.

This website utilizes technologies such as cookies to enable essential site functionality, as well as for analytics, personalization, and targeted advertising. You may change your settings at any time or accept the default settings. You may close this banner to continue with only essential cookies. [Privacy Policy](#)

[Manage Preferences](#)

[Accept All](#)

[Reject All](#)